ACS OMEGA

http://pubs.acs.org/journal/acsodf

Article

Cadmium-Free Nanostructured Multilayer Thin Films with Bright Blue Photoluminescence and Excellent Stability

Kai Ou,* Jia Luo, Shenwei Wang, Lixin Yi, and Yudong Xia*

Cite This: *ACS Omega* 2021, 6, 16869−16875

Read Online

ACCESS | Metrics & More | Article Recommendations

ABSTRACT: Cadmium-based quantum dots (Cd-QDs) show decent performance for lighting applications due to good color saturation, an excellent high quantum yield, and a narrow full-width at half-maximum. However, the intrinsic toxicity of Cd is a major hindrance to related applications, especially in the biological field. ZnSe, with a band gap of 2.7 eV and lower toxicity than CdSe or CdS, is promising as a blue luminescent material. Herein, we mainly reported the preparation and luminescence properties of nanostructured ZnSe/ZnS multilayer thin films with bright blue photoluminescence. The photoluminescence spectrum contained two emission peaks, located at about 442 nm (near band-edge emission) and 550 nm (defect-related emission), respectively. More importantly, the photoluminescence performance and decay were explored in detail through low-temperature photoluminescence spectra. In addition, the nanostructured ZnSe/ZnS multilayer thin films showed favorable photostability.

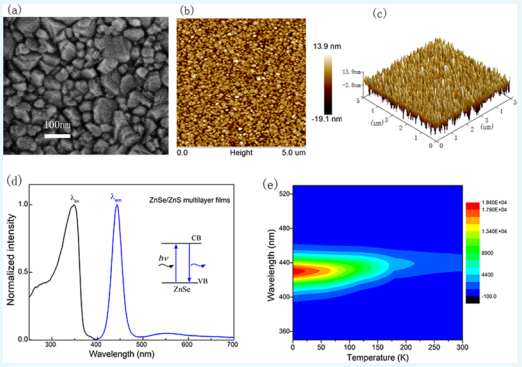

1. INTRODUCTION

Colloidal quantum dots (QDs),[1] with narrow band emissions and high photoluminescence (PL) quantum yields, are considered as next-generation candidates in the field of luminescence and display. Especially, the emission spectra of QDs can cover the whole visible range conveniently by controlling compositions or particle sizes. In the last two decades, many different structures, such as single-core, core/shell, and core/multishell structures, have been studied for photovoltaic applications. Among these research studies, Cd-based quantum dots occupied the vast majority, like CdS QDs,[2] $CdS_{1-x}Se_x$ QDs,[3] CdS/ZnS core/shell QDs,[4] CdTe/CdS/ZnS core/shell/shell QDs,[5] etc. However, the intrinsic toxicity of Cd is a major obstacle in the biological field. So, it is extremely necessary and significant to seek a new alternative Cd-free material or put forward some new nanostructures with better luminous performance.

ZnSe, with a wide band gap of about 2.7 eV[6] in the bulk material and much less toxicity than CdSe or CdS, has been identified as a promising blue-light-emitting material to replace ZnO. Based on the properties of a wide band gap and excellent luminescence efficiency, ZnSe has been widely used in transistors,[7] lasers,[8] solar cells,[9] photodetectors,[10] blue-light-emitting diodes,[11] etc. In addition, unlike ZnO, ZnSe is also reported as a p- and n-type semiconductor, although it is still more difficult to realize an effective p-type than n-type ZnSe semiconductor.[12] Till date, various ZnSe nanostructures have been investigated,[13−16] and many different methods have also been reported to prepare ZnSe films, such as chemical bath deposition,[17] magnetron sputtering,[18] coprecipitation method,[19] molecular beam epitaxy,[20] thermal evaporation,[21] electrodeposition,[22] pulsed laser deposition technique,[23] and electron-beam evaporation.[24] Among these preparation methods, electron-beam evaporation has the advantages of economy of materials, convenient operation, and environmental friendliness.

Here, we mainly reported the preparation and optical properties of nanostructured ZnSe/ZnS multilayer thin films, which were deposited by electron-beam evaporation. During the preparation, many detailed parameters could be controlled accurately, including the deposition rate, thickness, substrate temperature, etc. The heterostructured film showed bright blue photoluminescence. In this structure, ZnSe acts as a luminescent layer and ZnS acts as a passivation layer,[25,26] respectively. For better understanding, a variety of properties of heterostructured multilayer films, crystal structure, morphology, excitation spectra, photoluminescence, and fluorescence lifetimes were studied. Especially, the mechanism of photoluminescence decay was explored through low-temperature PL. Furthermore, it was also found that the heterostructured

Received: March 19, 2021
Accepted: June 11, 2021
Published: June 23, 2021

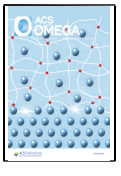

ZnSe/ZnS multilayer thin films show favorable photostability, which is attributed to the stability of the pure inorganic structure.

2. RESULTS AND DISCUSSION

2.1. Crystal Structures. Figure 1 demonstrates the X-ray diffraction (XRD) patterns of annealed heterostructured multilayer thin films. It can be observed that the diffraction peaks (002), (110), and (112) of ZnS are located at 2θ = 28.5, 47.5, and 56.4°, respectively, and the orientations (111), (200), and (220) of ZnSe are located at 2θ = 27.3, 31.5, and 45.2°, respectively. The XRD peaks agree well with the cubic structure of ZnSe and the wurtzite structure of ZnS, which are consistent with the values of JCPDS:88-2345 and JCPDS:79-2204, respectively. In addition, some other weakened crystallization peaks exist, which are derived from the Si substrate. Therefore, it is concluded that the annealed multilayer thin films have good crystalline quality. What is more, the mutually independent peaks indicate that ZnSe and ZnS do not form a mixing structure in these kinds of nanostructured multilayer thin films. Based on the broadening of corresponding X-ray spectral peaks, the average crystallite size of the nanostructured films can be estimated using Debye Scherrer's formula[17]

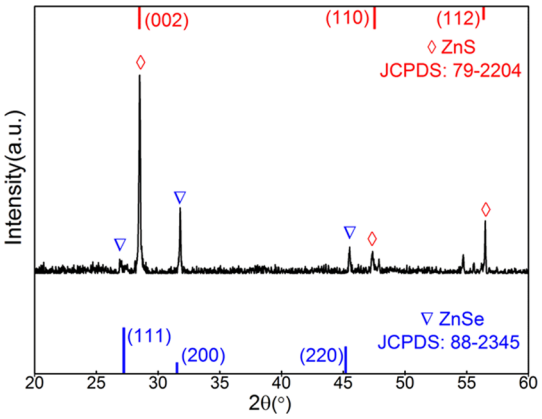

Figure 1. XRD patterns of the heterostructured multilayer thin films.

$$D = k\lambda/\beta \cos\theta \quad (1)$$

where k is the Scherrer constant equal to 0.89, λ is the X-ray wavelength of Cu Kα that is 0.154 nm, θ is the Bragg diffraction angle, $\beta = \sqrt{\beta_{obs}^2 - \beta_{std}^2}$ represents the structural broadening, and β_{obs} and β_{std} are the integral X-ray peak profile width of the sample and the standard of silicon, respectively. The average crystal size of the annealed nanostructured sample is about 69 nm through Debye Scherrer's formula.

2.2. Surface Morphologies. Surface morphologies play a vital role in understanding the growth surface and surface roughness of the films. Figure 2 shows the scanning electron microscopy (SEM) micrographs and atom force microscopy (AFM) images of the annealed nanostructured films. Figure 2a,b shows the surface and cross-sectional images, respectively. It can be seen from Figure 2a that uniform and well-defined grains cover the surface of a substrate completely, indicating that the annealed nanostructured multilayer films have good crystal quality. A film of uniform thickness covered on the Si substrate is shown in Figure 2b. In addition, Figure 2c,d shows the two-dimensional (2D) and three-dimensional (3D) AFM images, respectively. It is revealed that the multilayer thin films possess uniform and smooth morphologies. The root-mean-square roughness is about 4.73 nm, which indicates that the annealed nanostructured multilayer films' surface is quite smooth. The smooth surface morphology is in favor of the performance of the films and the devices. In general, all results from the surface morphologies provide further evidence for good crystal quality.

XPS is also an important tool for characterizing the compositions and structures of nanomaterials. Figure 3 shows the typical XPS survey spectra of annealed multilayer films in the whole binding energy region. We can observe that

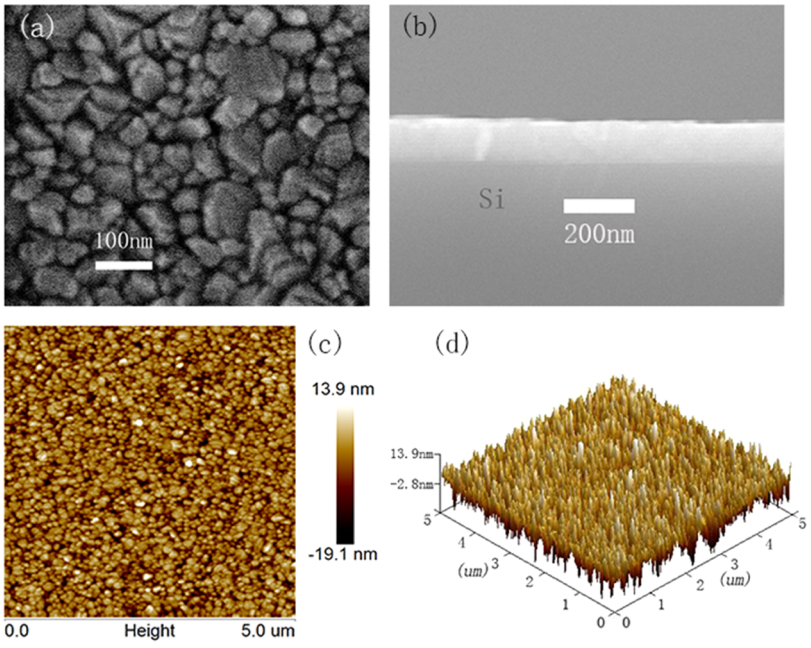

Figure 2. Surface (a) and cross-sectional (b) SEM images and AFM images (c and d) of the annealed films.

https://doi.org/10.1021/acsomega.1c01481
ACS Omega 2021, 6, 16869−16875

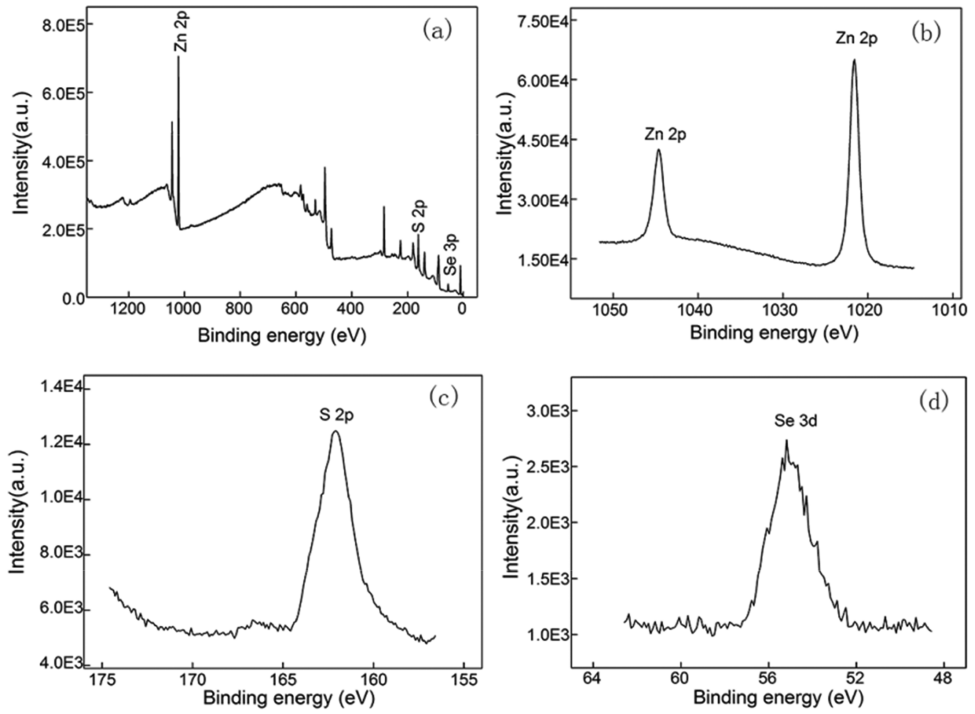

Figure 3. Typical XPS spectra of annealed nanostructured multilayer thin films (a). The detailed spectra of Zn 2p (b), S 2p (c), and Se 3d (d), respectively.

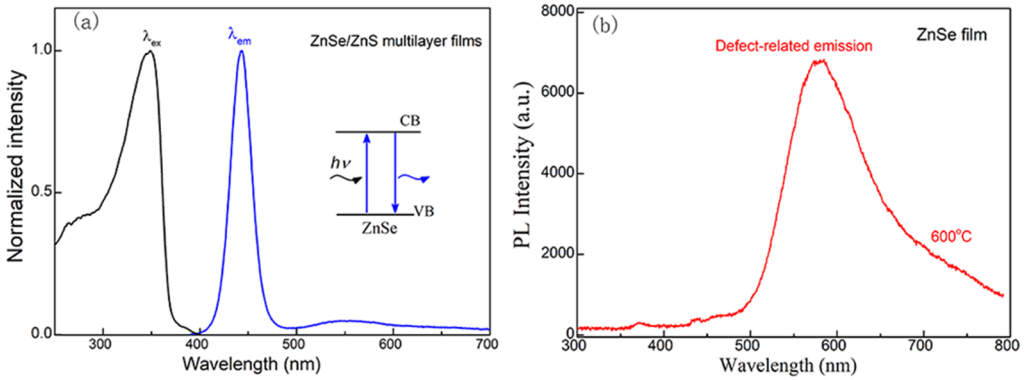

Figure 4. PLE and PL spectra of nanostructured ZnSe/ZnS multilayer thin films (a), and the PL spectrum of the bare ZnSe film (b).

the distinct Zn 2p, S 2p, and Se 3d peaks are located at 1021.59, 162.09, and 55.07 eV, respectively. It is consistent with the results of other nanostructured ZnSe/ZnS core/shell QDs[28] and ZnSSe alloy nanorods.[29] Hence, these XPS spectra further validate the formation of nanostructured ZnSe/ZnS multilayer thin films. In addition, the oxygen peak is located at 531.0 eV in the XPS survey spectrum, as shown in Figure 3a, which likely belongs to the chemisorbed oxygen. Due to the annealed nanostructured films without the strict packaging treatment, some chemisorbed oxygen could be adsorbed in air; especially, ZnS materials have strong water absorption.

2.3. Optical Properties. Then, we studied the luminescent properties of the nanostructured multilayer films and the bare ZnSe film, as shown in Figure 4. Both the photoluminescence excitation (PLE) and PL spectra were measured at room temperature. It can be observed from Figure 4a that PL emission spectra contain two peaks centered at 442 nm (2.81 eV) and 550 nm (2.25 eV), respectively. The high-intensity emission peak (full-width at half-maximum (FWHM) ≈ 27 nm) comes from the near band-edge (NBE) emission of ZnSe. Compared with the NBE emission of bulk ZnSe located at about 460 nm (2.7 eV), it shows a distinct blue shift by 20 nm. In our heterostructured multilayer films, the thickness of each ZnSe layer is approximately 3 nm, which is less than its Bohr exciton radius (about 4.5 nm[30]). So, we propose that this blue shift of the near band-edge emission is resulted from quantum confinement in a nanostructure. The weak and wide emission peak corresponds to defect-related (DL) emission, including Se and S vacancies and lattice and structure defects.[31] However, only a strong emission located at about 580 nm can be obtained for the bare ZnSe film, as shown in Figure 4b. This is mainly due to the Se vacancy caused by the loss of Se in the annealing process. It can be concluded that the presence of ZnS can suppress the defects and is beneficial to obtaining the NBE emission of ZnSe in these nanostructured multilayer films.

The PL decay spectrum showing in Figure 5 was measured. It could be well fitted through a triple exponential function

https://doi.org/10.1021/acsomega.1c01481
ACS Omega 2021, 6, 16869−16875

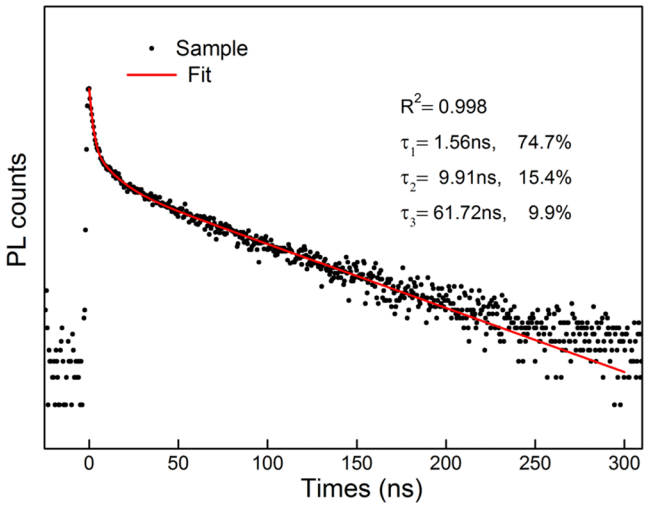

Figure 5. PL decay and corresponding fitting curves of multilayer thin films.

$$I(t) = A_1 \exp(-t/\tau_1) + A_2 \exp(-t/\tau_2) + A_3 \exp(-t/\tau_3) \quad (2)$$

It gives three PL lifetimes τ_1 = 1.56 ns, τ_2 = 9.91 ns, and τ_3 = 61.72 ns, with a percentage of 74.7, 15.4, and 9.9%, respectively. It is reported that the short lifetime of τ_1 originates from exciton recombination, and τ_2 can be attributed to the high trap density resulted from the surface of a crystal, while τ_3 comes from the carrier recombination in a defect-free bulk crystal.[32] Therefore, it is concluded that the fluorescence decay of annealed heteronanostructured multilayer films proceeds predominantly by exciton radiative recombination.

In addition, low-temperature PL spectra were used to further analyze the mechanism of PL decay in our nanostructured multilayer films. Figure 6 shows the temperature-dependent PL

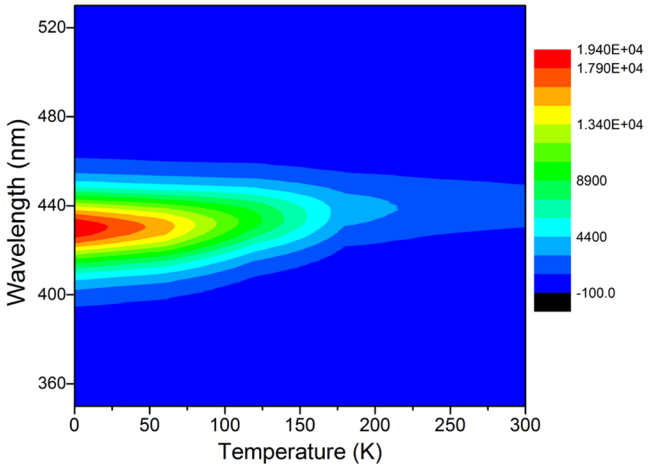

Figure 6. Pseudocolor maps of low-temperature PL spectra, and the color represents the PL intensity.

pseudocolor maps under different low-temperature conditions. It is observed that the PL intensity increases prominently as temperature decreases. The nonradiative Auger recombination has been reported in core/thick-shell nanocrystals,[33] and the Auger process is one of the main factors in decreasing PL intensity.[34] According to the current literature studies, the relationship between the temperature and conduction or valence band offsets is unclear. The valence band offsets are always positive at least 400 meV.[35] Therefore, regardless of the temperature in the heterostructure, the holes are always limited in the core, and we only need to consider the position of the electrons. As shown in Figure 7, Auger processes are

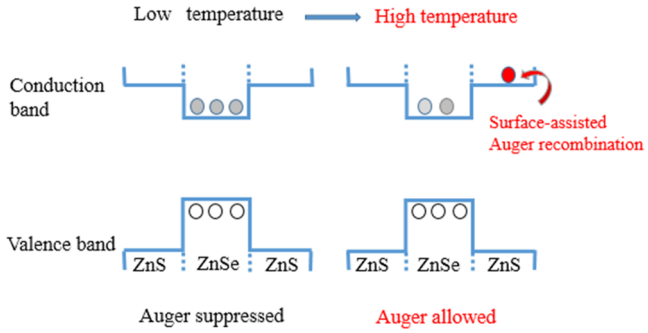

Figure 7. Schematic diagram of temperature-dependent electron localization.

prohibited when all of the electrons are in the ground state of ZnSe at low temperatures. However, Auger processes are allowed when some electrons are delocalized in ZnS at high temperatures.[33] Therefore, we suggest that the recombination of defects is enhanced and more photogenerated carriers are involved in the nonradiative process when the temperature increases, which leads to more phonons being generated and dissipated by means of thermal radiation. As a result, the total number of photons decreases, eventually resulting in a reduction of radiation transitions and the PL intensity.

With the changing temperature T, the PL intensity $I_{PL}(T)$ can be described as the following formula reported by Li et al.[36]

$$I_{PL}(T) = I_0 \times \frac{K_r(T)}{K_r(T) + K_{nr}(T)} \quad (3)$$

where I_0 is the T_0 corresponding PL peak intensity, we use T = 10 K as the benchmark, and $K_r(T)$ and $K_{nr}(T)$ are the recombination rates of radiative and nonradiative processes related to temperature, respectively. The recombination rate of nonradiative $K_{nr}(T)$ is determined by the rates of defect trap and the electron relaxation in the conduction or the valence band. The value of $K_{nr}(T)$ increases to some extent as the temperature elevates. Therefore, the increase of NBE emission is attributed to the reduction of nonradiative processes at low temperatures (Figure 6).

To further research the exciton binding energy, the relationship between the PL intensity and temperature can be determined using the following equation[37]

$$I(T) = \frac{I_0}{1 + A \exp(-E_b/k_B T)} \quad (4)$$

where the Boltzmann constant k_B is 1.38×10^{-23} J/K, I_0 is the PL intensity at 0 K, and E_b is the exciton binding energy. Based on the fitting analysis showing in Figure 8, the E_b value of the annealed nanostructured multilayer thin films is about 78.4 meV. Larger exciton binding has been reported to indicate potentially higher photoluminescence intensity.

Figure 9 describes the variation trend of the position and FWHM of NBE emission at different temperatures. As the temperature decreases, a significant blue shift of the peak

https://doi.org/10.1021/acsomega.1c01481
ACS Omega 2021, 6, 16869−16875

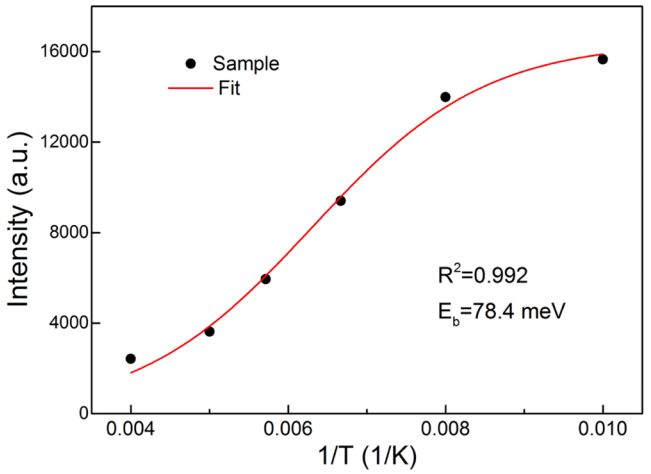

Figure 8. Fitting curve of exciton binding energy of multilayer thin films.

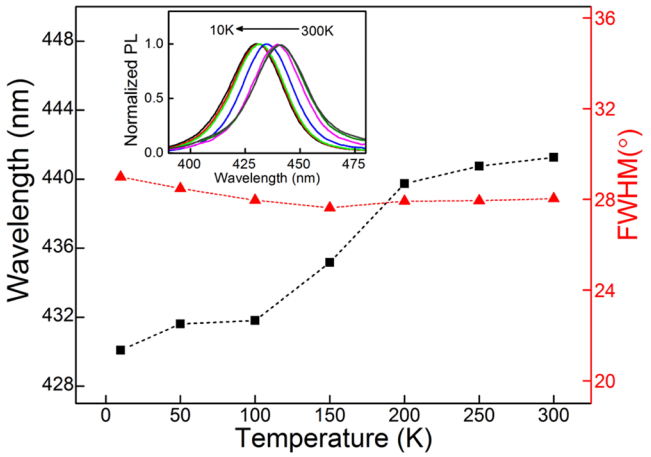

Figure 9. Variation trend of the position and FWHM of NBE emission at different temperatures from 300 to 10 K. The inset shows normalized PL spectra.

position can be observed. The blue-shift phenomenon at low temperature is attributed to the lattice contraction and quantum confinement. However, the FWHM of NBE emission without much variation is about 27 nm. As the temperature decreases, the increasing PL intensity and the blue shift of NBE emission can be analyzed using the Varshni formula[38]

$$\Delta E_g(T) = \frac{\alpha T^2}{\beta + T} \tag{5}$$

$$\Delta E_g(T) = E_g(T = 0) - E_g(T) \tag{6}$$

where $\Delta E_g(T)$ is the difference of energy band between two temperatures, α is the entropy, and β is the Debye temperature. We can get the dependence between temperature and the energy band as follows

$$E_g(T) = E_g(10) + \frac{\alpha 10^2}{\beta + 10} - \frac{\alpha T^2}{\beta + T} \tag{7}$$

It can be seen from formula 7 that the band gap E_g increases with decreasing temperature. The reduction in the E_g value is due to the weakening of electronic phonon interactions and the lattice shrinkage at low temperatures. Therefore, the blue shift of near band-edge emission occurs from 300 to 10 K.

What is more, according to the photon energy formula

$$E = h\nu = hc/\lambda \tag{8}$$

It can also be concluded that a larger energy band leads to enhanced light and shorter wavelength emission at lower temperatures.

2.4. Stability Analysis. The stability of luminescence performance has a great impact on its application. We placed the annealed nanostructured films in a valve bag to isolate the dust and then placed the bag in the air, without the strict packaging treatment like organic materials and devices. After a period of time, a PL test was performed. The results are shown in Figure 10. It can be observed that the annealed nanostructured ZnSe/ZnS multilayer thin films still maintained excellent luminous intensity after 2 years. This slight

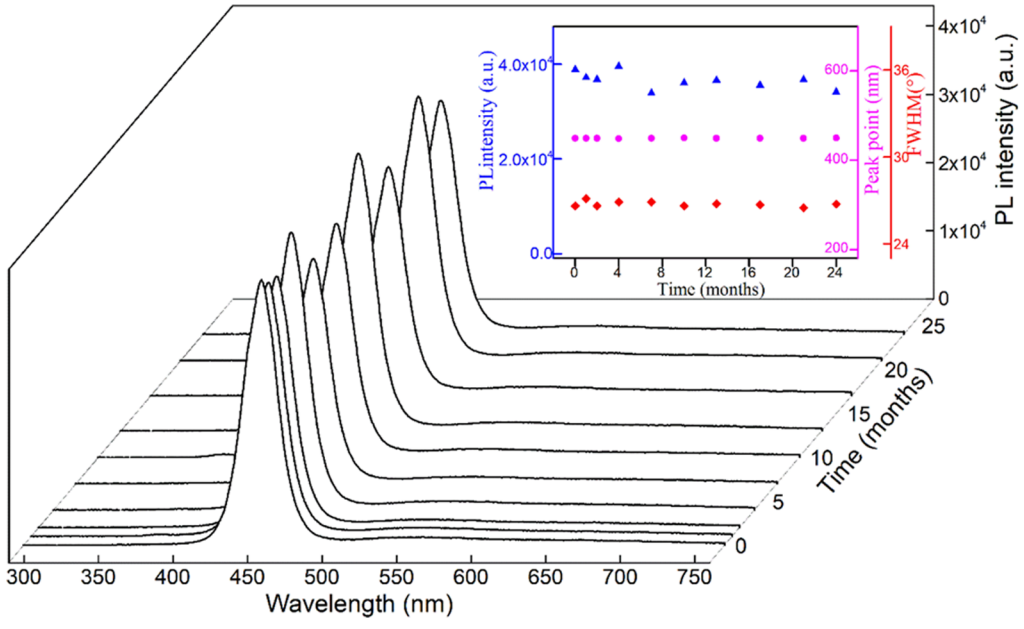

Figure 10. PL spectra of the sample at set intervals. The inset shows the changing trend of the PL intensity, peak point, and FWHM.

https://doi.org/10.1021/acsomega.1c01481
ACS Omega 2021, 6, 16869−16875

fluctuation in the PL intensity may be due to the deviation of spectrometer intensity or the test position. The peak point and FWHM of the NBE emission hardly changed. In short, these cadmium-free nanostructured ZnSe/ZnS multilayer thin films have bright blue photoluminescence and excellent stability in air.

3. CONCLUSIONS

In summary, we presented nanostructured ZnSe/ZnS multilayer thin films with bright blue photoluminescence and excellent stability. It was found that the annealed nanostructured films consisted of cubic zincblende ZnSe and wurtzite ZnS with good crystal quality. The PL spectrum located at about 442 and 550 nm corresponds to the NBE emission of ZnSe and DL emission, respectively. In addition, through the low-temperature PL spectra from 300 to 10 K, the increasing intensity of NBE emission and the blue shift of the peak position were observed. The increasing PL intensity was due to the weakening of the Auger process and the nonradioactive process at low temperatures. The analysis of PL decay revealed that the fluorescence decay was predominantly resulted from exciton radiative recombination. In addition, bright blue photoluminescence and excellent stability in air were confirmed.

4. EXPERIMENTAL SECTION

4.1. Preparation of Nanostructured Films. The nanostructured multilayer films were alternately deposited on a silicon substrate by electron-beam evaporation (EVA450). Both the purchased ZnSe and ZnS particles with a purity of 99.99% were used as starting materials without any treatment. The silicon substrate was cleaned with acetone, alcohol, and deionized water, successively. Since the conditions such as thickness and annealing temperature have been reported in detail in our previous work,[27] we chose the optimal preparation conditions. In simple terms, the vacuum degree of the cavity was kept at about 2.0×10^{-3} Pa during the deposition process. A quartz crystal monitor was used to monitor the deposition rate and thickness of the films. The thickness of the ZnSe layer was 3 nm with a growth rate of 0.5−0.6 Å/s, and the ZnS layer was 14 nm thick with a growth rate of 0.8−1.0 Å/s. At last, 10 layers of each ZnS and ZnSe of equal thicknesses were alternately deposited, and the total number of layers is 20. Finally, the deposited films were annealed in a quartz tube full of nitrogen (N_2) at 660 °C for 100 min to improve the crystal quality of the films. In addition, a monolayer ZnSe film was deposited on the Si substrate for contrasting purposes and annealed at 600 °C due to the appearance of cracks in the ZnSe film at more than 600 °C.

4.2. Characterization Techniques. The annealed nanostructured film samples were characterized for further study. The crystalline phases were tested by X-ray diffraction (XRD) measurements. All of the photoluminescence excitation (PLE) spectra, low-temperature PL spectra, and time-resolved PL spectra were measured with a fluorescence spectrometer (FLS920), where a 450 W xenon lamp was used as an excitation source. PL stability measurement was investigated by a CCD spectrometer, in which a 325 nm He−Cd laser was employed as an excitation source. Furthermore, the surface morphology and roughness of the nanostructured films were investigated by scanning electron microscopy (SEM) and atom force microscopy (AFM), respectively. X-ray photoelectron spectroscopy (XPS) was carried out to further explore the compositions and surface properties of nanostructured materials. All tests were performed at room temperature, except for low-temperature PL spectra.

AUTHOR INFORMATION

Corresponding Authors

Kai Ou − *School of Physical Science and Technology, Southwest Jiaotong University, Chengdu 610031, China*; orcid.org/0000-0002-1770-4819; Email: oukai@swjtu.edu.cn

Yudong Xia − *School of Physical Science and Technology, Southwest Jiaotong University, Chengdu 610031, China*; Email: Ydxia@swjtu.edu.cn

Authors

Jia Luo − *School of Physical Science and Technology, Southwest Jiaotong University, Chengdu 610031, China*

Shenwei Wang − *Key Laboratory of Luminescence and Optical Information, Ministry of Education, Institute of Optoelectronic Technology, Beijing Jiaotong University, Beijing 100044, China*

Lixin Yi − *Key Laboratory of Luminescence and Optical Information, Ministry of Education, Institute of Optoelectronic Technology, Beijing Jiaotong University, Beijing 100044, China*

Complete contact information is available at: https://pubs.acs.org/10.1021/acsomega.1c01481

Author Contributions

All authors contributed equally to this work.

Notes

The authors declare no competing financial interest.

ACKNOWLEDGMENTS

This work was financially supported by the Fundamental Research Funds for the Central Universities (A0920502052101-100 and A0920502052101-103) and the National Science Foundation of China (Grant no. 61975008).

REFERENCES

(1) Evans, C. M.; Cass, L. C.; Knowles, K. E.; Tice, D. B.; Chang, R. P.; Weiss, E. A. Review of the synthesis and properties of colloidal quantum dots: the evolving role of coordinating surface ligands. *J. Coord. Chem.* **2012**, *65*, 2391−2414.

(2) Moloney, M. P.; Gun'ko, Y. K.; Kelly, J. M. Chiral highly luminescent CdS quantum dots. *Chem. Commun.* **2007**, *38*, 3900−3902.

(3) Chen, Z.; Peng, W.; Zhang, K.; Zhang, J.; Yanagida, M.; Han, L. Surface ion transfer growth of ternary CdS 1−x Se x quantum dots and their electron transport modulation. *Nanoscale* **2012**, *4*, 7690−7697.

(4) Steckel, J. S.; Zimmer, J. P.; Coe-Sullivan, S.; Stott, N. E.; Bulović, V.; Bawendi, M. G. Blue luminescence from (CdS) ZnS core−shell nanocrystals. *Angew. Chem., Int. Ed.* **2004**, *43*, 2154−2158.

(5) He, Y.; Lu, H. T.; Sai, L. M.; Su, Y. Y.; Hu, M.; Fan, C. H.; Huang, W.; Wang, L. H. Microwave synthesis of water-dispersed CdTe/CdS/ZnS core-shell-shell quantum dots with excellent photostability and biocompatibility. *Adv. Mater.* **2008**, *20*, 3416−3421.

(6) Desai, H. N.; Dhimmar, J. M.; Modi, B. P. Optical and Dispersion Analysis of Zinc Selenide Thin Film. *Mater. Today: Proc.* **2016**, *3*, 1650−1657.

(7) Chiu, M.-Y.; Chen, C.-C.; Sheu, J.-T.; Wei, K.-H. An optical programming/electrical erasing memory device: Organic thin film

transistors incorporating core/shell CdSe@ ZnSe quantum dots and poly (3-hexylthiophene). *Org. Electron.* **2009**, *10*, 769−774.
(8) Sennaroglu, A.; Demirbas, U.; Vermeulen, N.; et al. Continuous-wave broadly tunable Cr2+: ZnSe laser pumped by a thulium fiber laser[J]. *Opt. Commun.* **2006**, *268*, 115−120.
(9) Huang, F.; Zhang, L.; Zhang, Q.; Hou, J.; Wang, H.; Wang, H.; Peng, S.; Liu, J.; Cao, G. High Efficiency CdS/CdSe Quantum Dot Sensitized Solar Cells with Two ZnSe Layers. *ACS Appl. Mater. Interfaces* **2016**, *8*, 34482−34489.
(10) Chang, S.-J.; Lin, T.; Su, Y.-K.; Chiou, Y.; Wang, C.; Chang, S.; Chang, C.; Tang, J.; Huang, B. Homoepitaxial ZnSe MSM photodetectors with various transparent electrodes. *Mater. Sci. Eng. B* **2006**, *127*, 164−168.
(11) Kim, Y.-H.; Lee, S. Y.; Song, W.; Ryu, D. H.; Meng, M.; Kim, W. Y.; Wood, R.; et al. High contrast blue organic light-emitting diodes using inorganic multilayers of Al and ZnSe. *Opt. Lett.* **2012**, *37*, 5235−5237.
(12) Su, Q.; Zhang, Y.; Li, S.; Du, L.; Zhao, H.; Liu, X.; Li, X. Synthesis of p-type phosphorus doped ZnSe nanowires and their applications in nanodevices. *Mater. Lett.* **2015**, *139*, 487−490.
(13) Park, H.; Chung, H.; Kim, W. Synthesis of ultrathin wurtzite ZnSe nanosheets. *Mater. Lett.* **2013**, *99*, 172−175.
(14) Li, L. S.; Pradhan, N.; Wang, Y.; Peng, X. High quality ZnSe and ZnS nanocrystals formed by activating zinc carboxylate precursors. *Nano Lett.* **2004**, *4*, 2261−2264.
(15) Chate, P. A.; Sathe, D. J.; Hankare, P. P. Growth and characteristics of Zn−Se−S thin layers by dip method. *J. Alloys Compd.* **2011**, *509*, 9425−9427.
(16) Yousefi, R.; Azimi, H. R.; Mahmoudian, M. R.; Basirun, W. J. The effect of defect emissions on enhancement photocatalytic performance of ZnSe QDs and ZnSe/rGO nanocomposites. *Appl. Surf. Sci.* **2018**, *435*, 886−893.
(17) Thirumavalavan, S.; Mani, K.; Sagadevan, S. A study of structural, morphological, optical and electrical properties of Zinc Selenide (ZnSe) thin film. *Mater. Today: Proc.* **2016**, *3*, 2305−2314.
(18) Vivet, N.; Morales, M.; Levalois, M.; Charvet, S.; Jomard, F. Optimization of the structural, microstructural and optical properties of nanostructured Cr2+: ZnSe films deposited by magnetron co-sputtering for mid-infrared applications. *Thin Solid Films* **2010**, *519*, 106−110.
(19) Bigdeli Tabar, M.; Elahi, S. M.; Ghoranneviss, M.; Yousefi, R. Controlled morphology of ZnSe nanostructures by varying Zn/Se molar ratio: the effects of different morphologies on optical properties and photocatalytic performance. *CrystEngComm* **2018**, *20*, 4590−4599.
(20) Hsiao, C. H.; Chang, S. J.; Wang, S. B.; Hung, S. C.; Chang, S. P.; Li, T. C.; Lin, W. J.; Huang, B. R. MBE growth of ZnSe nanowires on oxidized silicon substrate. *Superlattices Microstruct.* **2009**, *46*, 572−577.
(21) Mahesha, M. G.; Rashmitha; Meghana, N.; Padiyar, M. Investigation of effect of annealing on thermally evaporated ZnSe thin films through spectroscopic techniques. *Phys. B* **2017**, *520*, 37−42.
(22) Gromboni, M. F.; Mascaro, L. H. Optical and structural study of electrodeposited zinc selenide thin films. *J. Electroanal. Chem.* **2016**, *780*, 360−366.
(23) Williams, J. E.; Camata, R. P.; Fedorov, V. V.; Mirov, S. B. Pulsed laser deposition of chromium-doped zinc selenide thin films for mid-infrared applications. *Appl. Phys. A* **2008**, *91*, 333−335.
(24) Ou, K.; Wang, S.; Wan, G.; Zhang, X.; Duan, X.; Yi, L. Structural, morphological and optical properties of ZnO films by thermal oxidation of ZnSe films. *Thin Solid Films* **2017**, *634*, 51−55.
(25) Molaei, M.; Bahador, A. R.; Karimipour, M. Green synthesis of ZnSe and core−shell ZnSe@ZnS nanocrystals (NCs) using a new, rapid and room temperature photochemical approach. *J. Lumin.* **2015**, *166*, 101−105.
(26) Hofman, E.; Robinson, R. J.; Li, Z. J.; Dzikovski, B.; Zheng, W. Controlled Dopant Migration in CdS/ZnS Core/Shell Quantum Dots. *J. Am. Chem. Soc.* **2017**, *139*, 8878−8885.
(27) Ou, K.; Wang, S.; Huang, M.; Zhang, Y.; Wang, Y.; Duan, X.; Yi, L. Influence of thickness and annealing on photoluminescence of nanostructured ZnSe/ZnS multilayer thin films prepared by electron beam evaporation. *J. Lumin.* **2018**, *199*, 34−38.
(28) Ma, R.; Zhou, P.-J.; Zhan, H.-J.; Chen, C.; He, Y.-N. Optimization of microwave-assisted synthesis of high-quality ZnSe/ZnS core/shell quantum dots using response surface methodology. *Opt. Commun.* **2013**, *291*, 476−481.
(29) Park, S.; Kim, H.; Jin, C.; Lee, C. Synthesis, structure, and photoluminescence properties of ZnSSe alloy nanorods. *Curr. Appl. Phys.* **2012**, *12*, 499−503.
(30) Zhang, Q.; Li, H.; Ma, Y.; Zhai, T. ZnSe nanostructures: Synthesis, properties and applications. *Prog. Mater. Sci.* **2016**, *83*, 472−535.
(31) Zedan, I. T.; Azab, A. A.; El-Menyawy, E. M. Structural, morphological and optical properties of ZnSe quantum dot thin films. *Spectrochim. Acta, Part A* **2016**, *154*, 171−176.
(32) Leng, M.; Chen, Z.; Yang, Y.; Li, Z.; Zeng, K.; Li, K.; Niu, G.; He, Y.; Zhou, Q.; Tang, J. Lead-Free, Blue Emitting Bismuth Halide Perovskite Quantum Dots. *Angew. Chem., Int. Ed.* **2016**, *55*, 15012−15016.
(33) Javaux, C.; Mahler, B.; Dubertret, B.; Shabaev, A.; Rodina, A. V.; Efros, A. L.; Yakovlev, D. R.; Liu, F.; Bayer, M.; Camps, G.; Biadala, L.; Buil, S.; Quelin, X.; Hermier, J. P. Thermal activation of non-radiative Auger recombination in charged colloidal nanocrystals. *Nat. Nanotechnol.* **2013**, *8*, 206−212.
(34) Shen, Y. C.; Mueller, G. O.; Watanabe, S.; Gardner, N. F.; Munkholm, A.; Krames, M. R. Auger recombination in InGaN measured by photoluminescence. *Appl. Phys. Lett.* **2007**, *91*, No. 141101.
(35) Steiner, D.; Dorfs, D.; Banin, U.; Della Sala, F.; Manna, L.; Millo, O. Determination of band offsets in heterostructured colloidal nanorods using scanning tunneling spectroscopy. *Nano Lett.* **2008**, *8*, 2954−2958.
(36) Li, H.; Zhu, X.; Tang, Z. K.; Zhang, X. H. Low-temperature photoluminescence emission of monolayer MoS 2 on diverse substrates grown by CVD. *J. Lumin.* **2018**, *199*, 210−215.
(37) Zhang, J.; Yang, Y.; Deng, H.; Farooq, U.; Yang, X.; Khan, J.; Tang, J.; Song, H. High Quantum Yield Blue Emission from Lead-Free Inorganic Antimony Halide Perovskite Colloidal Quantum Dots. *ACS Nano* **2017**, *11*, 9294−9302.
(38) Zhang, X.; Chua, S.; Yong, A.; Yang, H.; Lau, S.; Yu, S.; Sun, X.; Miao, L.; Tanemura, M.; Tanemura, S. Exciton radiative lifetime in ZnO nanorods fabricated by vapor phase transport method. *Appl. Phys. Lett.* **2007**, *90*, No. 013107.

https://doi.org/10.1021/acsomega.1c01481
ACS Omega 2021, 6, 16869−16875